Numerical linked-cluster expansions for disordered lattice models

M. D. Mulanix,[1,2] Demetrius Almada,[1] and Ehsan Khatami[1]

[1]*Department of Physics and Astronomy, San Jose State University, San Jose, California 95192, USA*
[2]*Department of Physics, Rice University, Houston, Texas 77005, USA*

Imperfections in correlated materials can alter their ground state as well as finite-temperature properties in significant ways. Here, we develop a method based on numerical linked-cluster expansions for calculating exact finite-temperature properties of disordered lattice models directly in the thermodynamic limit. We show that a continuous distribution for disordered parameters can be achieved using a set of carefully chosen discrete modes in the distribution, which allows for the averaging of properties over all disorder realizations. We benchmark our results for thermodynamic properties of the square-lattice Ising and quantum Heisenberg models with bond disorder against Monte Carlo simulations and study them as the strength of disorder changes. We also apply the method to the disordered Heisenberg model on the frustrated checkerboard lattice, which is closely connected to $Sr_2Cu(Te_{0.5}W_{0.5})O_6$. Our method can be used to study finite-temperature properties of other disordered quantum lattice models, including those for interacting lattice fermions.

I. INTRODUCTION

Disorder, caused in materials by lattice defects, distortions, or impurities, can have profound effects on the properties of many-body systems. Even though noninteracting systems experiencing disorder-driven Anderson localization [1] have fascinated scientists for decades, it is the interplay of disorder and correlations that has attracted much attention in recent years, mostly in the context of many-body localization [2–4], including with site disorder in quantum spin models both theoretically [5,6] and experimentally [7–9]. The phenomenon is characterized by the absence of thermalization and the breakdown of conventional statistical physics descriptions of isolated systems.

Quenched bond disorder in magnetic models (affecting the exchange interactions) can result in frustration and glassy behavior [10,11], characterized by freezing of spins in random directions over macroscopic times below a critical freezing temperature. Short-range cases were first studied in the mid-1970s [12–14], when, for example, the effect of increasing the concentration of ferromagnetic bonds with fixed strengths in an antiferromagnetic nearest-neighbor Ising model on the critical temperature was explored. More recently, bond disorder in quantum spin models was also associated with the formation of gapless spin liquids in frustrated geometries [15–21].

In this work, we focus on the exact thermodynamic properties of disordered magnetic models away from their ground state. We employ the numerical linked-cluster expansion (NLCE) [22,23], which has been broadly used to study exact finite-temperature properties of magnetic as well as itinerant electron models in the thermodynamic limit [24–26], and develop an algorithm that allows it to be used for disordered lattice models with continuous random distributions. A method to solve lattice models with *bimodal* disorder within the NLCE was discussed in Refs. [27,28]. The authors

demonstrated that such systems can be solved exactly through averaging of properties of finite clusters over all of their 2^N disorder realizations, where N is the cluster size. In other words, in this approach full averaging is used to restore the translational symmetry of the lattice model, a necessary condition for the most common formulation of the NLCE.

The generalization of the above technique to continuous random distributions of a model parameter within the NLCE is not straightforward. A typical numerical approach for a disordered system with continuous uniform or nonuniform disorder involves averaging of properties over a large enough number of disorder realizations with randomly chosen parameters. Such a sampling scheme would, in principle, introduce statistical errors in the final properties whose magnitude depends on the strength of the disorder, the system size, the physics of the model, and the property under investigation. Such errors hinder the NLCE calculations and can lead to huge rounding errors in the eventual contribution of clusters to the series and, in turn, a rapid loss of convergence.

Here, we approach the problem of continuous disorder in the NLCE while trying to maintain the exact nature of the calculations. We do this by (1) extending the idea for the bimodal disorder to a *multimodal* disorder and (2) allowing disorder modes to be distributed nonuniformly. For point (1), any distribution of a random model parameter is replaced by a discrete distribution consisting of m modes so that, if m is a small enough integer, the full disorder average over the m^N realizations can still be performed on any cluster in the series up to a practical order. On the other hand, point (2) allows for a careful choice of the mode locations that results in a fast convergence of properties to the continuous disorder limit by increasing m in our discrete formalism. It is accomplished here by choosing the mode locations such that moments of our discrete distribution match those of the continuous one for each m.

For example, when $m = 2$, the locations of the two modes, x_1 and x_2, in a box distribution centered around zero are determined through the knowledge of the first two moments of the distribution; the first moment is zero, which means $x_2 = -x_1$. The second moment is $\Delta^2/3$, where Δ is the half width of the box, and, when equated with the second moment of our discrete distribution $x_{1,2}^2$, yields unique $x_{1,2}$. Since all the odd moments of such a symmetric distribution are zero, it may be more efficient, however, to work with absolute moments instead. This is discussed in Sec. III B, where the mode values up to $m = 8$ are calculated.

Applying the technique to the classical Ising and quantum Heisenberg models on the square lattice, we demonstrate this fast convergence by showing that a typical $m \leqslant 6$ can already provide results that are valid for the random disorder at temperatures accessible to the NLCE. We study the thermodynamic properties of these models for several bond disorder strengths and compare our data to those obtained from Monte Carlo (MC) simulation of finite-size clusters. We then employ the method to study properties of the disordered Heisenberg model on the frustrated checkerboard lattice that could be relevant to recent experiments on $Sr_2Cu(Te_{1-x}W_x)O_6$ [19–21]. Our method paves the way for exploring the exact finite-temperature properties of disordered quantum lattice models, including those of interacting fermions, directly in the thermodynamic limit.

II. MODELS

A. Two-dimensional Ising model

The Hamiltonian of the random-bond Ising model on the square lattice is written as

$$H^{\text{Ising}} = \sum_{\langle i,j \rangle} J_{ij} S_i^z S_j^z, \tag{1}$$

where $\langle i, j \rangle$ denotes that i and j are nearest neighbors, $J_{ij} = J + R_{ij}$, with our choice of $J = 1$ being the unit of energy, R_{ij} is a random number drawn from either a uniform box distribution in $[-\Delta, \Delta]$ or a normal distribution with standard deviation Δ, and S_i^z represents the z component of a spin $1/2$ at site i. The clean system $J_{ij} = J$ ($\Delta = 0$) has a continuous phase transition at a finite temperature to the magnetically ordered phase. With our choice of parameters, the transition takes place at $T = 1/2\ln(1 + \sqrt{2}) \sim 0.57$.

B. Two-dimensional Heisenberg model

The Hamiltonian of the random-bond quantum Heisenberg model is written as

$$H^{\text{Heis}} = \sum_{i,j} J_{ij} \mathbf{S}_i \cdot \mathbf{S}_j, \tag{2}$$

where $\mathbf{S}_i$ is the spin-$1/2$ vector at site i. Despite the lack of a continuous phase transition at nonzero temperatures according to the Mermin-Wagner theorem [29], the clean version of the Heisenberg model on the square lattice (nonzero J_{ij} for only nearest-neighbor bonds) develops strong antiferromagnetic correlations below the temperature $T \sim 0.6$ signaled by a peak in the specific heat as a function of temperature. Unlike the classical Ising model, the Heisenberg model does not have

the $J_{ij} \rightarrow -J_{ij}$ symmetry. On the checkerboard lattice, the next-nearest-neighbor exchange interactions are nonzero on every other 2×2 plaquette.

III. METHODS

A. The NLCE algorithm

The numerical linked-cluster expansion is a method in which a given extensive property $P(\mathscr{L})$ is expressed as a sum over the contributions to that property from every cluster that can be embedded in the lattice $\mathscr{L}$. This series expansion is

$$P(\mathscr{L}) = \sum_c W_P(c), \tag{3}$$

where c is a cluster that can be embedded in $\mathscr{L}$ and $W_P(c)$ is the corresponding contribution to property P and is computed through the inclusion-exclusion principle:

$$W_P(c) = P(c) - \sum_{s \subset c} W_P(s), \tag{4}$$

where s is a cluster that can be embedded in c (a subcluster of c) and $P(c)$ for finite clusters up to a certain size are calculated using exact diagonalization (ED).

The true power of the method is demonstrated in the thermodynamic limit where $\mathscr{L} \rightarrow \infty$. In that limit, we would be interested in the property per site, $\lim_{\mathscr{L} \rightarrow \infty} P(\mathscr{L})/\mathscr{L}$, which can be obtained by considering contributions only from those clusters that are not related by translational symmetry on the right-hand side of Eq. (3). More simplifications are made by combining contributions from clusters that are topologically or symmetrically the same given the Hamiltonian and the lattice geometry under investigation. Details of the algorithm can be found in Ref. [23].

B. Random disorder

In an expansion for disordered systems, cluster properties $P(c)$ are replaced by those averaged over disorder realizations, as is done in Refs. [27,28,30] for bimodal disorder, leading to disorder-averaged contributions and, ultimately, the disorder-averaged property in the thermodynamic limit. In the case of bimodal disorder, the disorder average could be taken exactly; ED was performed on all disorder realizations of every cluster in the series, and hence, no statistical errors were introduced. The latter is crucial for the NLCE since any small error in the properties of clusters, especially in low orders, can be amplified via the subcluster subtraction in Eq. (4), rendering $P(\mathscr{L})$ useless. The conventional treatment of continuous disorder in numerical methods, namely, an ensemble average of properties over a large number of random realizations, has also been tried using the NLCE in one dimension to study the onset of many-body delocalization through the calculation of area-law entanglement [31]. The disorder average for this specific property could be done on $P(\mathscr{L})$, after the NLCE sums were performed for a given realization, to avoid rounding errors due to the statistical noise. That is because only a finite number of clusters crossing a bipartitioning boundary contributed to the series in each order even in the presence of disorder. In other words, breaking the translational symmetry

of the lattice by introducing disorder did not greatly affect the number of clusters to be diagonalized in each order.

The main idea of this paper is to extend the exact treatment of disorder within the NLCE for a *generic* property to the limit of continuous random distributions by systematically increasing the number of disorder "modes" in a multimodal implementation of the discrete disorder distribution. One may be tempted to keep increasing the number of modes m on an equally spaced grid in the range $[-\Delta, \Delta]$, for example, for the box disorder and study the convergence of the disorder-averaged properties as $m \to \infty$. However, the number of realizations grows as m^N in the exact treatment of such a disorder, and one finds that the convergence in this case is slow to the point that the limit of continuous disorder remains inaccessible for most quantum lattice models of interest.

This problem can be mitigated through an efficient choice of locations of the disorder modes in the range, so that the discrete distribution and the continuous distribution of interest share as many moments as possible. This is motivated by the fact that any physical distribution can be fully realized based on the knowledge of its moments. The nth moment is defined as $\frac{1}{2\Delta} \int_{-\Delta}^{\Delta} x^n dx$ for the continuous distribution and $\frac{1}{m} \sum_{i=1}^{m} x_i^n$ for the discrete distribution, where x_i is the location of the ith mode. However, in this formulation, the odd moments are zero by symmetry, so we restrict ourselves to the moments of only the right half of the distributions and consider a mode value of zero (at the center of the disorder box) for an odd number of modes. We then obtain the negative modes by multiplying x_i on the positive side by a minus sign. Hence, to calculate m mode values, one would need to equate $\text{int}(m/2)$ of the absolute moments:

$$\frac{1}{m} \sum_{i=1}^{m} |x_i^n| = \frac{1}{\Delta} \int_0^\Delta x^n dx = \frac{\Delta^n}{1+n} \qquad (5)$$

for $n = 1, \ldots, \text{int}(m/2)$. Note that to avoid double counting the zero mode, we average the absolute value of x_i^n over the entire box on the left-hand side of the above equation.

This yields $x_{1,2} = \pm\Delta/2$ for the bimodal disorder; by choosing the two modes to be at 50% of Δ on each side of the box, as opposed to at $\pm\Delta$, one can already obtain an approximation for the case of continuous box disorder. For $m = 3$, we choose $x_2 = 0$. The left-hand side of Eq. (5) for $n = 1$ will then be $\frac{2}{3}|x_{1,3}|$, and the right-hand side will be $\frac{1}{2}\Delta$, and hence, $x_{1,3} = \pm\frac{3}{4}\Delta$. For a larger number of modes, Eq. (5) will be a set of nonlinear equations for x_i, which may be solved numerically. Figure 1 shows the location of modes for $\Delta = 1$ up to $m = 5$. In Table I, we have listed the mode locations up to $m = 8$, which is the maximum used in our study.

Our method of finding an efficient set of disorder modes in the approach to the continuous distribution is not unique. One may come up with alternative ways of implementing a multimodal distribution. For example, the location of the modes in the box can be fixed to integer fractions of Δ, while their "strengths" are calculated through the matching of the moments with the continuous distribution in a procedure similar to that above.

The disorder-averaging process adds significant computation time to the NLCE. However, the introduction of disorder often leads to localization effects, which in turn result in a
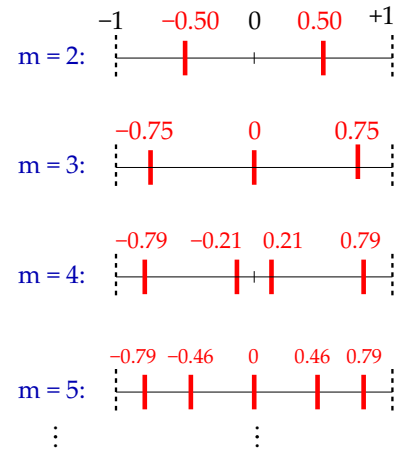

FIG. 1. Locations of the discrete disorder modes used in the NLCE for a box distribution that extends from -1 to 1. m denotes the number of modes. For a given m, the locations are determined by matching an appropriate number of moments of the discrete distribution on the positive half of the box with those of the original continuous box distributions. See text for details.

faster convergence of the NLCE at a given temperature. On the other hand, we find that with the above choice of modes, the convergence in m is very quick for a Δ of the order of J. In practice, $m \lesssim 6$ is generally sufficient for convergence to the continuous limit at temperatures where NLCE is converged. For these reasons, one can carry out the calculations to low enough temperatures for the disordered systems where useful comparisons to the clean system are practical.

IV. RESULTS

A. Ising model

As the first case study, we choose the two-dimensional (2D) Ising model with the uniform bond disorder described in Sec. II A. Since the computations do not involve any matrix diagonalization for this already diagonal model, we are able to carry out the series to very high orders for both the clean and disordered systems. Figure 2(a) shows the convergence of the series for the average energy E as a function of temperature T for several values of m from 2 to 8. It also shows results for the clean system. For the latter, the convergence is lost just before the transition temperature around $0.6J$. As the disorder with a strength of $\Delta = 1.5$ is introduced to the system, the sharp

TABLE I. Mode locations for the box distribution for up to eight modes.

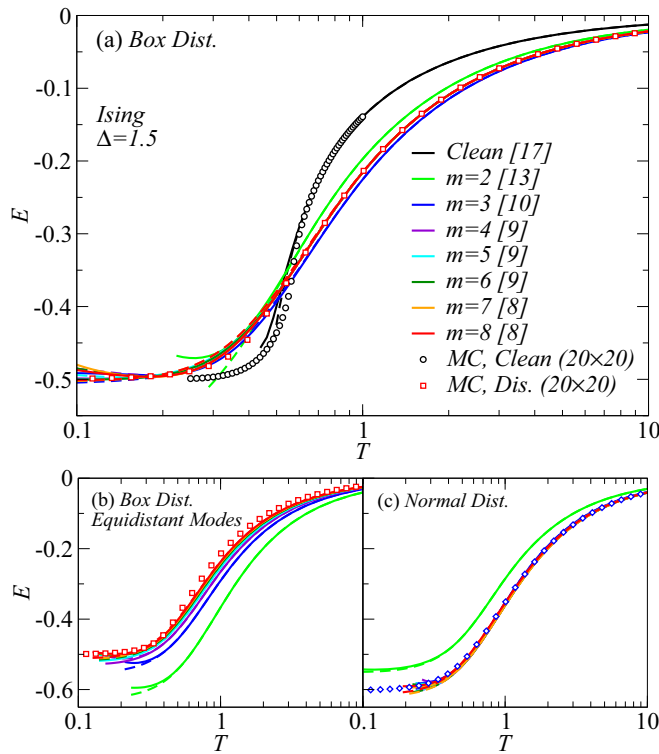| m	x_i			
2	±0.5000			
3	0.0000,	±0.7500		
4	±0.2113,	±0.7886		
5	0.0000,	±0.4636,	±0.7863	
6	±0.1470,	±0.4993,	±0.8537	
7	0.0000,	±0.4191,	±0.4346,	±0.8959
8	±0.1020,	±0.4095,	±0.5901,	±0.8982

FIG. 2. Average energy of the clean and disordered 2D Ising model from the NLCE in the thermodynamic limit vs temperature. The strength of the bond disorder is set to $1.5J$. The results for the disordered model are obtained using discrete distributions for the disorder with different numbers of modes m from 2 to 8. (a) and (b) correspond to box distributions, whereas (c) corresponds to the normal distribution. Mode locations in (a) and (c) are chosen based on criteria discussed in Sec. III B, while those in (b) are equidistant within the distribution box. In all cases, the next-to-last and last orders of the NLCE for each m are shown as dashed and solid lines, respectively. The largest order used in the series for each m is indicated inside square brackets in (a). Lines in (b) and (c) are the same as in (a), except that 11 orders are used for $m = 2$. We also show Monte Carlo results for a clean system of size 20×20 and for the continuous box (red squares) and normal (blue diamonds) distributions of disorder with the same disorder strength of $1.5J$ using the parallel tempering method. Error bars are smaller than the symbol sizes. In (a) and (c), the NLCE results rapidly converge to the limit of an infinite number of modes by increasing m to about 4, while in (b), even $m = 8$ is not sufficient to capture the exact results at high temperatures.

drop in the energy at the critical point disappears, and the series converges down to slightly lower temperatures between $0.4J$ and $0.5J$. Interestingly, with a larger m the last two orders of the series remain closer to each other to much lower temperatures. The calculations for each m are carried out to a maximum order that would require a few thousand hours of CPU time. As we increase m, we are forced to truncate the series at lower orders because of the m^N scaling, where N is the same as the order in our site expansion.

Figure 2(a) also demonstrates the rapid settlement of the energy curves to a final form with increasing m. The results for $m > 4$ and $T > 0.5$ are not distinguishable from those for
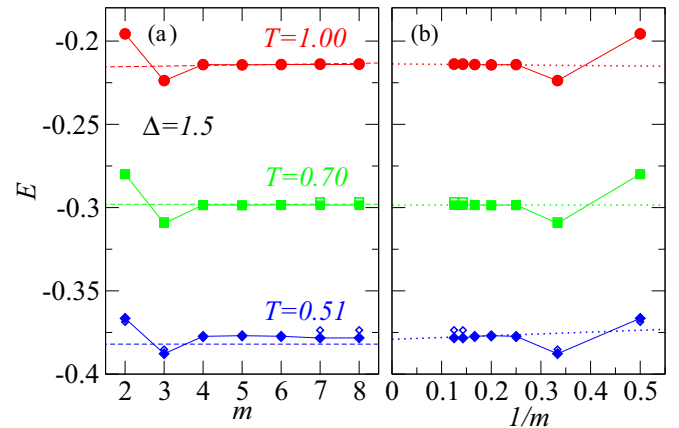

FIG. 3. Average energy of the disordered Ising model with $\Delta = 1.5J$ at fixed temperatures vs (a) the number of disorder modes m of the discrete disorder distribution and (b) $1/m$ from the NLCE. The data show fast convergence with m in all cases above the convergence temperatures of the series. To gauge the latter, we plot the last and next-to-last orders of the expansion for each case as solid and open symbols. Horizontal dashed lines in (a) are results from the Monte Carlo simulations for the continuous box disorder for a periodic 20×20 cluster with the same disorder strength. Dotted lines in (b) are linear fits to data for $m = 5$–8, except at $T = 0.51$, where $m = 5$ and 6 are used for the fit.

$m = 4$ in this figure. The convergence to the limit of random disorder is quickly reached. For comparison, we show results from a parallel tempering MC simulation with a 20×20 periodic cluster for both the clean and disordered systems. We have performed an average over 200 disorder realizations for the latter. There is very good agreement between the MC and NLCE results in the converged region of $T > 0.5$ and for $m \geqslant 4$. At lower temperatures, despite the lack of convergence, NLCE results from the last two orders of the series for each m also seem to capture the essential behavior of the energy.

In Fig. 2(b), we show that the trend in convergence as m increases is significantly different when modes are placed on an equidistant grid in the box distribution. Even with eight modes, the exact MC results cannot be recovered even at very high temperatures.

In order to demonstrate the applicability of our method to cases where the distribution is other than uniform, in Fig. 2(c) we use our criteria to find mode locations for the normal (Gaussian) distribution and redo the NLCE calculations for the disordered Ising model using these modes. Like for the case of uniform distribution, we find that here, the convergence to the continuous disorder, indicated by diamonds representing MC results, is quickly reached. The curves for $m > 2$ essentially coincide with each other.

To analyze the way in which results converge as a function of the number of disorder modes for the box distribution, we plot in Fig. 3 the energy for the disorder strength of $1.5J$ at three fixed temperatures as a function of m and $1/m$. Also plotted as dashed horizontal lines in Fig. 3(a) are the MC results. A rapid convergence to final values by increasing m is clear from these plots, although the series is not completely converged for $m = 7$ and 8 at $T = 0.51$. The NLCE results at the two highest temperatures shown also agree with the
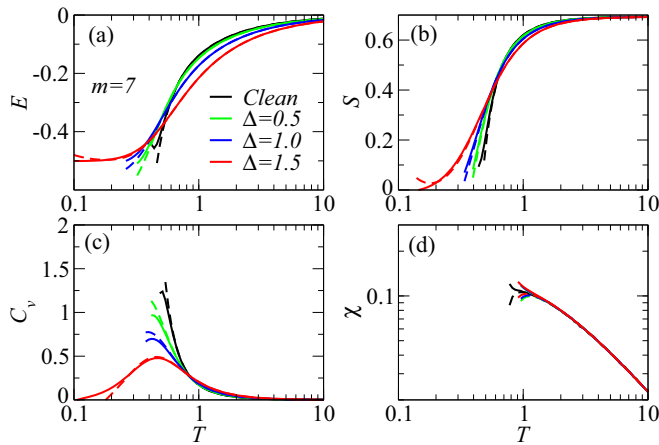
FIG. 4. Thermodynamic properties of the clean and disordered 2D Ising model from the NLCE vs temperature. The results for the disordered model with $\Delta = 0.5J$, $1.0J$, and $1.5J$ as labeled are for seven disorder modes ($m = 7$). The last two orders of the series are shown as dashed and solid lines. For $\Delta > J$ (red curves), the series for (a) the average energy, (b) entropy, and (c) specific heat converge to significantly lower temperatures than in the other two cases where $\Delta \leqslant J$ around $T = 0.2$. (d) The convergence and the values of the uniform susceptibility, however, are generally unaffected by the strength of the disorder strength in the range we have considered and follow those of the clean system.
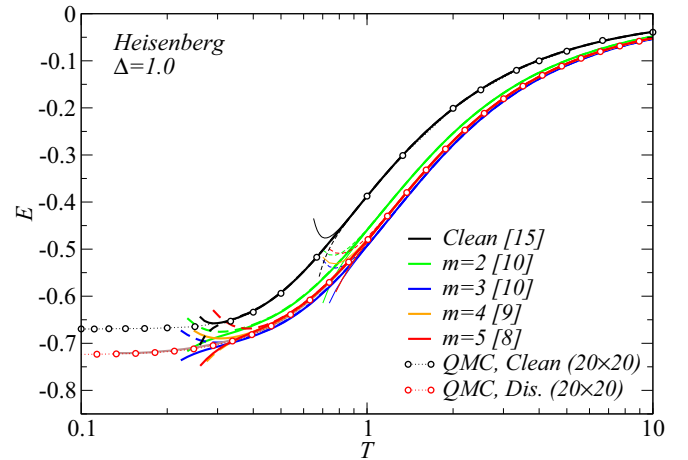

FIG. 5. Average energy of the clean and disordered 2D Heisenberg model in the thermodynamic limit vs temperature. The strength of the bond disorder for the latter is set to $1.0J$. Thin dashed and solid lines are the last two orders of the raw NLCE results for different numbers of disorder modes. The largest order used in the series for each m is indicated inside square brackets. Thick dashed and solid lines are results after numerical resummations; black and colored lines are the last two orders after the Euler resummation, and the brown line is the result after the Wynn resummation for $m = 4$. Convergence in the number of disorder modes is already achieved for this model with $m = 4$ above the lowest convergence temperature.

parallel tempering MC results within the statistical error bars of the latter. By performing MC simulations with systems sizes as large as 40×40, we have verified that the systematic finite-size error is small compared to the statistical errors at the temperatures we present. It is remarkable that the NLCE with clusters up to only eight sites can project what the average energy of the disordered system is in the thermodynamic limit with such high accuracy.

In Fig. 3(b), we fit the same results for the energy plotted as a function of $1/m$ to a line. We use values from the last four m for the fit, except at $T = 0.51$, where values for $m = 5$ and 6 are used due to a lack of convergence with $m = 7$ and 8. Such extrapolations to the $1/m = 0$ limit can be useful at low temperatures in cases where the convergence in m is not achieved while the convergence in the NLCE order is still present.

Having access to converged results for the disordered Ising model already with $m \sim 7$, we study next how the thermodynamics of the system are affected as the strength of the disorder Δ varies. In Fig. 4, we show the energy; the entropy $S = \ln Z + E/T$, where Z is the partition function; the heat capacity C_v obtained from fluctuations in the energy [32]; and the uniform spin susceptibility χ obtained from fluctuations in the magnetization as a function of temperature for $\Delta = 0.5$, 1.0, and 1.5. The disappearance of the divergence in the heat capacity for large Δ suggests that the second-order phase transition is washed away. Our model for Δ is closely related to the one studied by Pekalski and Oguchi [13] in which the increase in the probability of having ferromagnetic bonds in an antiferromagnetic Ising model leads to a rapid decrease in the critical temperature of the model. We also observe that the entropy of the disordered system decreases more gradually

as the temperature decreases, starting at higher temperatures in comparison to the clean system with no sign of a phase transition.

Interestingly, the susceptibility seems to be completely unaffected by disorder in the exchange constant regardless of its strength in the temperature region we have access to. The system with mostly antiferromagnetic tendencies is no more or less sensitive to ferromagnetic ordering with disorder. This is a fundamentally different behavior than that observed for bimodal disorder [27]. For the latter system, it was shown analytically and numerically that the corresponding susceptibility takes a simple $1/4T$ form as all the terms in the expansion except for the single site exactly vanish. However, an important distinction between the approach in Ref. [27] and ours (when $m = 2$) is that our disorder distribution for J is centered around its clean limit of 1, whereas Tang *et al.* used a bimodal distribution centered around 0.

B. Heisenberg model

To explore the effect of disorder and how the convergence of the series to the limit of uniform box disorder changes in the presence of quantum fluctuations, we study the disordered quantum Heisenberg model on the square lattice. We find that despite the increased complexity of the model in comparison to the Ising model and the fact that a smaller number of disorder modes can be considered due to the added computational cost for the diagonalization, the NLCE results converge to the limit of $m = \infty$ much more rapidly than for the classical Ising model. As can be seen in Fig. 5, for $\Delta = 1.0$ the average energy is converged with only four disorder modes
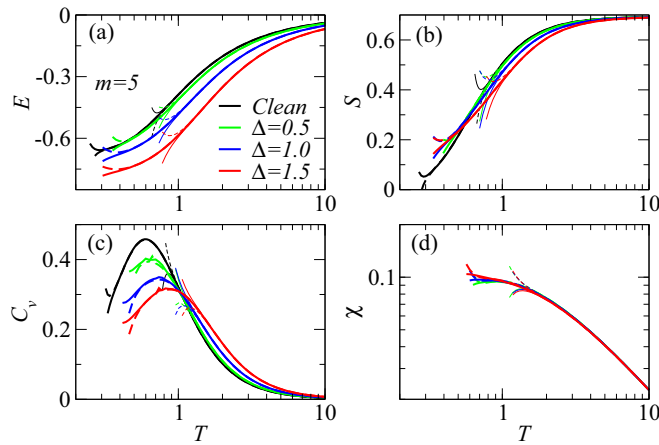
FIG. 6. (a) Average energy, (b) entropy, (c) specific heat, and (d) uniform susceptibility of the clean and disordered 2D Heisenberg model from the NLCE vs temperature. The results for the disordered model with $\Delta = 0.5J$, $1.0J$, and $1.5J$ as labeled are for five disorder modes ($m = 5$). Thin dashed and solid lines are the last two orders of the series. Thick dashed and solid lines are the results after the Euler and Wynn resummations, respectively.

at temperatures as low as $T \sim 0.4$. The results for $m = 5$ and $m = 6$ (the latter not shown) coincide with those for $m = 4$ in the above temperature range.

Here, the NLCE is generally carried out to lower orders for a given m than for the Ising model. We indicate the largest order in the square brackets in the legend of Fig. 5. However fortunately, we find that numerical resummations, such as the Euler and Wynn methods [23], typically used to extend the region of convergence of the NCLEs to lower temperatures, perform very well for this model. Figure 5 shows that the lowest convergence temperature decreases from $T \sim 1$ to $T = 0.3$–0.4 depending on m when resummations are used. To eliminate the possibility of introducing systematic errors through numerical resummations, we take the lowest convergence temperature to be the point at which results from the Euler and Wynn techniques agree with each other. Results from Euler and Wynn techniques are shown as thick lines in Fig. 5. We show that the results after resummations match those obtained from stochastic series expansion quantum Monte Carlo (QMC) simulations [33,34] of the model on a periodic 20×20 site cluster (see circles in Fig. 5). Interestingly, the results after the Wynn resummation for $m = 4$ (brown line) agree with those from the QMC down to a much lower temperature than what we can independently verify to be converged within the NLCE.

We find that the effect of disorder is felt generally more strongly and starting at higher temperatures in the Heisenberg model than in the Ising model. In Fig. 6, we show converged results for the disordered systems with $m = 5$ for three different disorder strengths. As soon as the strength becomes comparable to the average value for the exchange interaction, the energy deviates significantly from that in the clean limit starting at temperatures as high as 10. Unlike for the Ising model, we do not find a superior convergence in the series extending to much lower temperatures as the disorder strength increases to $\Delta = 1.5$, even with resummations. However, the

results point to a peak in the specific heat that gets suppressed and moves to higher temperatures as Δ increases. The peak, at least in the clean limit, marks the onset of short-range antiferromagnetic correlations developing in a system that lacks long-range order at finite temperatures.

In the disordered system the peak is likely associated with the freezing temperature (exceeding it by about 20% [11]). The shift to higher temperatures for such a tendency can be understood intuitively from the fact that, on average in the disordered system, half of the antiferromagnetic nearest-neighbor bonds are much stronger than the other half, which may also become ferromagnetic if $\Delta > J$. Having two bonds per site on a square lattice, the random configuration of weak and strong bonds can create a situation for spins to happily form dimers with neighbors they are most strongly coupled to and lower the entropy at higher temperatures at the expense of long-range Néel order at $T = 0$. The picture is similar to the "random-singlet" state proposed for the ground state of Heisenberg models with the same type of disorder as in our study but on frustrated lattices [15,16,18]. It is important to point out that $\Delta > J$ will lead to realizations that have a mix of antiferromagnetic and ferromagnetic bonds resulting in frustration, which complicates the QMC simulations due to the "sign problem" [35] and in turn limits its access to low temperatures.

Whether any nonzero Δ would be detrimental to the ground-state long-range order is an interesting question, which we cannot address with the present approach. It may be possible, however, to employ a zero-temperature NLCE with the Lanczos algorithm for the diagonalization step to explore ground-state properties, including the fate of the Néel order, starting in the limit of large Δ, where one may expect the series to converge at $T = 0$ due to the local nature of dimers, and gradually decreasing Δ. A similar idea was implemented to study the valence-bond solid to spin liquid transition of the pinwheel distorted kagome lattice Heisenberg model [36].

As a final case study we turn to the disordered frustrated Heisenberg model on the checkerboard lattice. We adopt the NLCE with a square expansion, where the building block is the corner-sharing 2×2 plaquette with crossed next-nearest-neighbor bonds as opposed to a single site; the order of the expansion indicates the maximum number of plaquettes used. We take both the nearest-neighbor (J) and the next-nearest-neighbor (J') exchange interactions to be 1. The geometry is also referred to as a planar pyrochlore lattice, and the thermodynamic properties of the Heisenberg model on it were previously studied extensively using the NLCE in the clean limit [37]. The model can be relevant to $Sr_2Cu(Te_{1-x}W_x)O_6$, where at $x = 0.5$ a "clean" version can be thought of as half of the plaquettes (Sr_2CuTeO_6) promoting Néel ordering while the other half (Sr_2CuWO_6), in a checkerboard pattern, promotes a columnar order. Both frustration and randomness seem to play important roles in the low-temperature properties, including possible spin liquid or columnar states [19–21]. There are several ways disorder can be introduced. For simplicity, we choose a random J' with a disorder strength of $\Delta_{J'} = 1.0$, leaving J intact [38]. We show the average energy and the specific heat vs temperature in Fig. 7. Similar to the unfrustrated square-lattice model, the convergence to the random disorder limit with increasing m is fast. The $m = 4$ and $m = 5$
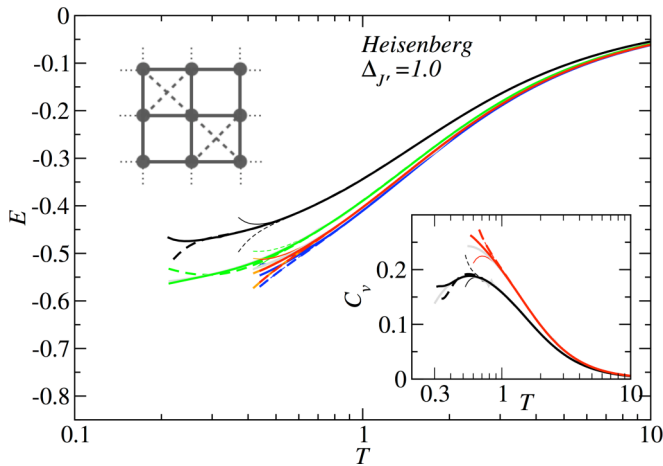
FIG. 7. Average energy and the specific heat (bottom inset) of the clean and disordered 2D Heisenberg model on the checkerboard lattice in the thermodynamic limit vs temperature. The average exchange interaction on all the bonds is set to $J = J' = 1.0$. The disorder with strength 1.0 is introduced to only the next-nearest-neighbor bonds. Lines are the same as in Fig. 5, except that the largest orders (numbers of squares) used in the series for the clean system and the disordered system with $m = 2, 3, 4$, and 5 are 6, 5, 4, 4, and 4, respectively. Results for the clean system are from Ref. [37]. The top inset shows a finite portion of the checkerboard lattice. Dashed lines denote J' on every other plaquette.

energy curves in the main panel are indistinguishable. Unlike in the case of the square lattice, here, the peak in the specific heat seems to rise as a result of disorder, signaling a reduction in frustration.

V. SUMMARY AND DISCUSSION

We have developed an algorithm within NLCEs that enables us to study disordered quantum lattice models with continuous disorder distributions. We have shown that the continuous limit can be approached using a multimodal discrete distribution scheme with an efficient choice for the mode locations and by systematically increasing the number of modes. The exact averaging of properties over all disorder realizations prevents the NLCE from breaking down due to statistical noise associated with random sampling from a continuous distribution, often used in numerical treatments of these systems, and allows one to obtain highly precise results for the disordered system in the thermodynamic limit. We show that despite the exponentially large number of disorder realizations that exist for every cluster in the series, the calculations remain feasible owing to the fact that the convergence to the continuous limit by increasing the number of modes is quite fast (between four and seven modes are necessary).

We applied this technique to the classical Ising model and the quantum Heisenberg model on the square lattice and stud-

ied their exact thermodynamic properties at finite temperatures as the strength of the disorder changes. We found that the effect of disorder is more prominent for the Heisenberg model in comparison to the Ising model at intermediate temperatures away from the critical region of the Ising model in the clean limit. While the uniform susceptibilities of both models were unaffected by disorder at our accessible temperatures, the specific heat of the Heisenberg model displays a shift in the location of the peak to higher temperatures, which we interpreted based on the promotion of random short-range antiferromagnetic dimer formations due to the existence of weak and strong bonds in the disordered system. We also applied the method to the disordered Heisenberg model on the frustrated checkerboard lattice, relevant to recent experiments on $Sr_2Cu(Te_{1-x}W_x)O_6$, and studied the effect of disorder in the next-nearest-neighbor bonds on the energy and heat capacity.

The idea for choosing the optimal location of the disorder modes based on moments of the distribution is not unique to the box distribution. As demonstrated, other deviates, such as a normal deviate for the disordered model parameters, often used in spin glass models, can be simulated using the NLCE following a procedure similar to that for the uniform distribution. The technique can be used to study other disordered quantum lattice models, such as the t-J and Hubbard models on the square lattice or other geometries. The method has great potential for models where the infamous sign problem [35,39] hinders QMC simulations. These will be the subject of our future studies.

NLCEs have been widely used to provide highly precise results for ultracold fermionic atoms in optical lattices [40–48]. The treatment of random disorder on the same footing as the Coulomb interactions in these fermionic systems can have great implications for experiments in which disorder can be simulated using optical speckles [49,50] or quasiperiodic potentials [51–53].

Finally, the use of faster solvers, such as the Lanczos algorithm for partial diagonalization, can be employed to access higher orders (and hence lower temperatures) without the loss of any information at currently accessible temperatures [54].

[1] P. W. Anderson, Phys. Rev. **109**, 1492 (1958).

[2] D. Basko, I. Aleiner, and B. Altshuler, Ann. Phys. (NY) **321**, 1126 (2006).

[3] V. Oganesyan and D. A. Huse, Phys. Rev. B **75**, 155111 (2007).

[4] D. M. Basko, I. L. Aleiner, and B. L. Altshuler, Phys. Rev. B **76**, 052203 (2007).

[5] M. Žnidarič, T. Prosen, and P. Prelovšek, Phys. Rev. B **77**, 064426 (2008).

[6] A. Pal and D. A. Huse, Phys. Rev. B **82**, 174411 (2010).

[7] J. Smith, A. Lee, P. Richerme, B. Neyenhuis, P. W. Hess, P. Hauke, M. Heyl, D. A. Huse, and C. Monroe, Nat. Phys. **12**, 907 (2016).

[8] K. X. Wei, C. Ramanathan, and P. Cappellaro, Phys. Rev. Lett. **120**, 070501 (2018).

[9] K. Xu, J.-J. Chen, Y. Zeng, Y.-R. Zhang, C. Song, W. Liu, Q. Guo, P. Zhang, D. Xu, H. Deng, K. Huang, H. Wang, X. Zhu, D. Zheng, and H. Fan, Phys. Rev. Lett. **120**, 050507 (2018).

[10] S. F. Edwards and P. W. Anderson, J. Phys. F **5**, 965 (1975).

[11] K. Binder and A. P. Young, Rev. Mod. Phys. **58**, 801 (1986).

[12] S. Katsura and F. Matsubara, Can. J. Phys. **52**, 120 (1974).

[13] A. Pekalski and T. Oguchi, Prog. Theor. Phys. **54**, 1021 (1975).

[14] F. Matsubara and M. Sakata, Prog. Theor. Phys. **55**, 672 (1976).

[15] K. Watanabe, H. Kawamura, H. Nakano, and T. Sakai, J. Phys. Soc. Jpn. **83**, 034714 (2014).

[16] H. Kawamura, K. Watanabe, and T. Shimokawa, J. Phys. Soc. Jpn. **83**, 103704 (2014).

[17] T. Shimokawa, K. Watanabe, and H. Kawamura, Phys. Rev. B **92**, 134407 (2015).

[18] K. Uematsu and H. Kawamura, J. Phys. Soc. Jpn. **86**, 044704 (2017).

[19] O. Mustonen, S. Vasala, E. Sadrollahi, K. P. Schmidt, C. Baines, H. C. Walker, I. Terasaki, F. J. Litterst, E. Baggio-Saitovitch, and M. Karppinen, Nat. Commun. **9**, 1085 (2018).

[20] O. Mustonen, S. Vasala, K. P. Schmidt, E. Sadrollahi, H. C. Walker, I. Terasaki, F. J. Litterst, E. Baggio-Saitovitch, and M. Karppinen, Phys. Rev. B **98**, 064411 (2018).

[21] K. Uematsu and H. Kawamura, Phys. Rev. B **98**, 134427 (2018).

[22] M. Rigol, T. Bryant, and R. R. P. Singh, Phys. Rev. Lett. **97**, 187202 (2006).

[23] B. Tang, E. Khatami, and M. Rigol, Comput. Phys. Commun. **184**, 557 (2013).

[24] M. Rigol, T. Bryant, and R. R. P. Singh, Phys. Rev. E **75**, 061118 (2007).

[25] M. Rigol, T. Bryant, and R. R. P. Singh, Phys. Rev. E **75**, 061119 (2007).

[26] E. Khatami and M. Rigol, Phys. Rev. A **84**, 053611 (2011).

[27] B. Tang, D. Iyer, and M. Rigol, Phys. Rev. B **91**, 174413 (2015).

[28] B. Tang, D. Iyer, and M. Rigol, Phys. Rev. B **91**, 161109(R) (2015).

[29] N. D. Mermin and H. Wagner, Phys. Rev. Lett. **17**, 1133 (1966).

[30] R. R. P. Singh and S. Chakravarty, Phys. Rev. Lett. **57**, 245 (1986).

[31] T. Devakul and R. R. P. Singh, Phys. Rev. Lett. **115**, 187201 (2015).

[32] E. Khatami and M. Rigol, Phys. Rev. A **86**, 023633 (2012).

[33] A. W. Sandvik, Phys. Rev. B **59**, R14157 (1999).

[34] We have used the code by A. W. Sandvik, available at http://physics.bu.edu/~sandvik/programs/index.html, and have modified it to account for disorder in the bond strengths.

[35] P. Henelius and A. W. Sandvik, Phys. Rev. B **62**, 1102 (2000).

[36] E. Khatami, R. R. P. Singh, and M. Rigol, Phys. Rev. B **84**, 224411 (2011).

[37] E. Khatami and M. Rigol, Phys. Rev. B **83**, 134431 (2011).

[38] The randomness in $O_2Cu(O_{0.5}O_{0.5})O_6$ stems from the cation mixing Te/W, which may lend itself more to a random J_1-J_2 model. However, the development of a NLCE for the latter model is beyond the scope of this work and will be a topic of future studies.

[39] E. Y. Loh, J. E. Gubernatis, R. T. Scalettar, S. R. White, D. J. Scalapino, and R. L. Sugar, Phys. Rev. B **41**, 9301 (1990).

[40] R. A. Hart, P. M. Duarte, T. L. Yang, X. Liu, T. Paiva, E. Khatami, R. T. Scalettar, N. Trivedi, D. A. Huse, and R. G. Hulet, Nature (London) **519**, 211 (2015).

[41] L. W. Cheuk, M. A. Nichols, K. R. Lawrence, M. Okan, H. Zhang, E. Khatami, N. Trivedi, T. Paiva, M. Rigol, and M. W. Zwierlein, Science **353**, 1260 (2016).

[42] M. F. Parsons, A. Mazurenko, C. S. Chiu, G. Ji, D. Greif, and M. Greiner, Science **353**, 1253 (2016).

[43] J. H. Drewes, E. Cocchi, L. A. Miller, C. F. Chan, D. Pertot, F. Brennecke, and M. Köhl, Phys. Rev. Lett. **117**, 135301 (2016).

[44] P. T. Brown, D. Mitra, E. Guardado-Sanchez, P. Schauß, S. S. Kondov, E. Khatami, T. Paiva, N. Trivedi, D. A. Huse, and W. S. Bakr, Science **357**, 1385 (2017).

[45] A. Mazurenko, C. S. Chiu, G. Ji, M. F. Parsons, M. Kanász-Nagy, R. Schmidt, F. Grusdt, E. Demler, D. Greif, and M. Greiner, Nature (London) **545**, 462 (2017).

[46] D. Mitra, P. T. Brown, E. Guardado-Sanchez, S. S. Kondov, T. Devakul, D. A. Huse, P. Schauß, and W. S. Bakr, Nat. Phys. **14**, 173 (2017).

[47] J. H. Drewes, L. A. Miller, E. Cocchi, C. F. Chan, N. Wurz, M. Gall, D. Pertot, F. Brennecke, and M. Köhl, Phys. Rev. Lett. **118**, 170401 (2017).

[48] M. A. Nichols, L. W. Cheuk, M. Okan, T. R. Hartke, E. Mendez, T. Senthil, E. Khatami, H. Zhang, and M. W. Zwierlein, Science **363**, 383 (2019).

[49] M. Pasienski, D. McKay, M. White, and B. DeMarco, Nat. Phys. **6**, 677 (2010).

[50] S. S. Kondov, W. R. McGehee, W. Xu, and B. DeMarco, Phys. Rev. Lett. **114**, 083002 (2015).

[51] M. Schreiber, S. S. Hodgman, P. Bordia, H. P. Lüschen, M. H. Fischer, R. Vosk, E. Altman, U. Schneider, and I. Bloch, Science **349**, 842 (2015).

[52] P. Bordia, H. P. Lüschen, S. S. Hodgman, M. Schreiber, I. Bloch, and U. Schneider, Phys. Rev. Lett. **116**, 140401 (2016).

[53] T. Kohlert, S. Scherg, X. Li, H. P. Lüschen, S. D. Sarma, I. Bloch, and M. Aidelsburger, Phys. Rev. Lett. **122**, 170403 (2019).

[54] K. Bhattaram and E. Khatami, arXiv:1810.06202.